HHS Public Access

Author manuscript

Nature. Author manuscript; available in PMC 2014 January 18.

Published in final edited form as:

Nature. 2013 July 18; 499(7458): 364–368. doi:10.1038/nature12232.

Carbon catabolite repression of the maltose transporter revealed by X-ray crystallography

Shanshuang Chen[1], **Michael L. Oldham**[2], **Amy L. Davidson**[3], and **Jue Chen**[1,2,*]

[1]Department of Biological Sciences, Purdue University, West Lafayette, IN 47907

[2]Howard Hughes Medical Institute, Purdue University, West Lafayette, IN 47907

[3]Department of Chemistry, Purdue University, West Lafayette, IN 47907

Summary

Efficient carbon utilization is critical to the survival of microorganisms in competitive environments. To optimize energy usage, bacteria have developed an integrated control system to preferentially uptake carbohydrates that support rapid growth. The availability of a preferred carbon source such as glucose represses the synthesis and activities of proteins necessary for the transport and metabolism of secondary carbon sources. This regulatory phenomenon is defined as carbon catabolite repression (CCR)[1]. In enteric bacteria, the key player of CCR is a component of the glucose-specific phosphotransferase system, enzyme IIA ($EIIA^{Glc}$)[1,2]. It is known that unphosphorylated $EIIA^{Glc}$ binds and inhibits a variety of transporters when glucose is available[1,2]. However, understanding the underlying molecular mechanism has been hindered by the complete absence of structures for any $EIIA^{Glc}$-transporter complexes. Here, we present the 3.9 Å crystal structure of $EIIA^{Glc}$ in complex with the maltose transporter, an ATP-binding cassette (ABC) transporter. The structure shows that two $EIIA^{Glc}$ molecules bind to the cytoplasmic ATPase subunits, stabilizing the transporter in an inward-facing conformation and preventing the structural rearrangements necessary for ATP hydrolysis. We also show that the half maximal inhibitory concentrations of the full-length $EIIA^{Glc}$ and an N-terminal truncation mutant differ by 60 fold, consistent with the hypothesis that the N-terminal region, disordered in the crystal structure, functions as a membrane-anchor to increase the effective $EIIA^{Glc}$ concentration at the membrane[3,4]. Together these data suggest a model of how the central regulatory protein $EIIA^{Glc}$ allosterically inhibits maltose uptake in *E. coli*.

Carbon catabolite repression (CCR) is common in bacteria and higher organisms; up to 5-10% of all bacterial genes are subject to CCR regulation[1]. Different organisms use different pathways to achieve CCR. In *E. coli*, CCR is mediated by the modulation of the

*To whom correspondence should be addressed (chenjue@purdue.edu).

Author Contributions: All authors designed the study and analyzed the data. S.C. crystallized the complex and performed the biochemical experiments. S.C. and M.L.O. determined the crystal structure and made the figures. J.C. wrote the manuscript with inputs from all authors.

Author Information: Coordinates and structure factors have been deposited in the Protein Data Bank under accession number 4JBW. The authors declare no competing financial interests.

phosphorylation state of the glucose-specific enzyme IIA ($EIIA^{Glc}$)[1,2]. $EIIA^{Glc}$ is a member of the phosphoenolpyruvate (PEP): carbohydrate phosphotransferase system (PTS) that transports and concomitantly phosphorylates several preferred carbohydrates[1,2]. The influx of PTS substrates and other readily metabolizable carbon sources increases the level of unphosphorylated $EIIA^{Glc}$ by affecting the intracellular [PEP]-[pyruvate] ratio[5]. Phosphorylated $EIIA^{Glc}$ stimulates cAMP synthesis[2], which leads to transcriptional activation of many catabolic genes. Unphosphorylated $EIIA^{Glc}$ directly inhibits several non-PTS sugar transport systems, including the maltose transporter ($MalFGK_2$), lactose permease (LacY), melibiose permease (MelB), and raffinose permease (RafB)[2]. It also prevents glycerol uptake by binding to the glycerol kinase, an enzyme key to glycerol metabolism[2]. These carbohydrates or their derivatives function as inducers to control the synthesis of the corresponding transporters and metabolic enzymes. Thus, interaction of $EIIA^{Glc}$ with the transporter not only directly prevents secondary carbon source uptake, but also down regulates the expression of the corresponding catabolic systems by reducing the intracellular level of the inducer[1,2]. The regulation of the *lac* operon is the best known example of this feedback mechanism called inducer exclusion[1,2]. The mechanisms of how $EIIA^{Glc}$ regulates target transporters have been studied for decades. Mutants of the lactose, maltose, raffinose, and melibiose permeases that abolish inducer exclusion have been isolated[2]. The interfaces between $EIIA^{Glc}$ and the target transporters have been probed biochemically[2]. While those studies have identified some of the residues involved in the interaction, no structure of any transporter in complex with $EIIA^{Glc}$ is yet available.

The maltose transporter $MalFGK_2$ belongs to the superfamily of ATP-binding cassette (ABC) transporters. It consists of two transmembrane (TM) subunits, MalF and MalG, and two copies of the ATPase subunits, MalK. The structure of MalK can be further divided into an N-terminal nucleotide binding domain (NBD) and a C-terminal regulatory domain (RD). Crystal structures of the maltose transporter have been determined in three distinct functional states. The inward-facing conformation, also known as the resting state in which the transporter has very low basal ATPase activity, was obtained in the absence of maltose and nucleotides[6]. The outward-facing conformation, corresponding to a hydrolysis competent intermediate, was stabilized by the periplasmic maltose-binding protein (MBP) and ATP[7]. Finally, a pre-translocation complex, which shows how substrate initiates the transport cycle, was captured in the presence of the MBP but in the absence of ATP[8]. These structures illustrate the coordinated motions of the transporter that couple ATP hydrolysis to maltose translocation[6-8]. On this foundation, the maltose transporter would be a productive system to study how sugar transport is regulated under conditions subject to inducer exclusion.

To obtain crystals of the maltose transporter bound with $EIIA^{Glc}$, we tested many constructs including full-length and truncated proteins devoid of flexible regions. It was unclear whether $EIIA^{Glc}$ binds to the transporter in the resting state or an intermediate conformation induced by MBP and/or ATP. Therefore, we carried out crystallization experiments with different combinations of cofactors. Crystals were obtained with full-length $MalFGK_2$ and $EIIA^{Glc}$ in the absence of MBP and ATP. Initially, the crystals obtained in detergent diffracted X-rays poorly (about 15 – 20 Å). Crystals grown in lipid/detergent bicelles

diffracted to 7 Å resolution. Dehydration caused the unit cell to shrink by 20 Å in one dimension and improved the resolution to 3.9 Å. The structure was determined by molecular replacement and refined with deformable elastic network (DEN) constraints (Table S1).

The asymmetric unit of the crystal contains two copies of the complex, each consisting of one transporter $MalFGK_2$ and two $EIIA^{Glc}$ molecules (Fig. 1). The maltose transporter shows a conformation similar to that of the resting state[6]. The root mean square deviation (rmsd) of the transporter (1,168 Cα positions, excluding flexible regions) between the resting state and the $EIIA^{Glc}$ complex structure is 2.2 Å (Fig. S1). In this conformation, the transmembrane maltose-binding site is exposed to the intracellular side of the membrane (inward-facing). In contrast to the resting state in which the periplasmic P2 loop is disordered, the structure of the P2 loop is well resolved (Fig. 1 and Fig. S2). The relative orientation of the P2 loop is different between the two structures in the asymmetric unit, likely influenced by crystal packing (Fig. S3 and Fig. S4). The two $EIIA^{Glc}$ molecules are bound at structurally equivalent positions, interacting exclusively with the intracellular MalK subunits. The $EIIA^{Glc}$-binding sites are distant from the Walker A motifs that bind ATP (Fig. 2a), the maltose-binding site in MalF, and the periplasmic loops to which maltose-MBP docks. Thus, $EIIA^{Glc}$ is a classical Monod-Wyman-Changeux (MWC) allosteric inhibitor of the maltose transporter[9].

The MalK subunits form an open dimer, interacting with each other through their C-terminal RD domains (Fig. 2a). Each $EIIA^{Glc}$ is wedged between the NBD of one MalK and the RD of the opposite MalK, linking these two domains together (Fig. 2a). Of the 1,500 $Å^2$ buried surface area on $EIIA^{Glc}$, approximately 55% is buried at the NBD interface and the other 45% at the RD interface. From this structure, it becomes apparent why binding of $EIIA^{Glc}$ would inhibit the maltose transporter. In contrast to the open dimer stabilized by $EIIA^{Glc}$, in the outward-facing state the two NBDs of MalK make contact with each other and two ATPs lie buried along the NBD interface (Fig. 2b). Superposition of the resting state and outward-facing structures shows that the conformational changes of MalK observed in the transport cycle are achieved principally by interdomain rotations of the NBDs relative to the RDs (Fig. 2b). In effect, the MalK subunits resemble a pair of tweezers, with the RDs acting as the fulcrum point allowing the two NBDs to open and close like the pincers[10]. Here we observe that by linking the NBD of one MalK with the opposite RD, the two $EIIA^{Glc}$ molecules fasten the tweezers in the open configuration. The two TM subunits MalF and MalG are docked onto the MalK NBDs, and conformational changes in the NBDs are tightly coupled to those of the TM domains[7] (Fig. 1 and Fig. 2). Thus, by preventing closure of the NBDs, $EIIA^{Glc}$ prevents the formation of the outward-facing conformation, a key step for ATP hydrolysis and maltose translocation. In excellent agreement with the crystal structure, all mutations that render resistance to $EIIA^{Glc}$ inhibition reside in the MalK subunit[11,12]. Among the eight mutations isolated, five make direct interactions with $EIIA^{Glc}$ in the crystal structure (Fig. 2c). The others, G278P, G302D, and S322F, are located in close proximity to the interface and likely produce local conformational changes that prevent $EIIA^{Glc}$ from binding (Fig. 2c).

The structure of $EIIA^{Glc}$ observed in the complex (residues 19-168) is very similar to that of the free form[13], with an overall rmsd of 0.5 Å. This reinforces the observation that neither

phosphorylation nor binding to target proteins induces substantial conformational changes of $EIIA^{Glc}$ [14-17]. As a central signaling molecule, $EIIA^{Glc}$ interacts with many proteins that share little sequence or structural similarity[2]. The NBD of MalK binds to a canonical surface of $EIIA^{Glc}$ that normally interacts with other partners (Fig. 2d, left). Of the 17 residues making contacts with the NBD, 11 are also involved in interacting with glycerol kinase, $EIIB^{Glc}$, and HPr[14-16] (Fig. 2d, left). The majority of the interface residues are hydrophobic, consistent with the promiscuous interactions this surface makes with different proteins. The crystal structure also shows why phosphorylation prevents the binding of $EIIA^{Glc}$ to the maltose transporter. The phosphorylation site His 90[18], located at the $EIIA^{Glc}$-MalK interface, is in its unphosphorylated form and Hydrogen bonded with Gln 122 of MalK (Fig. 2c). Adding a negatively charged phosphate group to the side chain of His 90 would disrupt the interface, thus relieving the maltose transporter from inducer exclusion. As previously suggested by antibody and peptide mapping experiments[19,20], residues contacting the RD are located away from the active site, forming an interface unique to the maltose transporter complex (Fig. 2d, right).

Although the N-terminal 18 residues of $EIIA^{Glc}$ are disordered in the crystal structure, data from other studies suggested that this region might still play an important role in stabilizing the $EIIA^{Glc}$-$MalFGK_2$ complex. Studies of synthetic peptides showed that residues 3-10 of $EIIA^{Glc}$ form an amphipathic helix in the presence of either detergent micelles or lipid vesicles (Fig. 3a), suggesting that it may function as a membrane anchor[3,4]. Furthermore, removing the N-terminal region of $EIIA^{Glc}$ hinders its interaction with membrane transporters, but not soluble partners[19,21-23]. In the $EIIA^{Glc}$-$MalFGK_2$ structure, $EIIA^{Glc}$ is oriented such that the N-terminus is pointed towards the membrane. The first ordered residue Thr 19 is approximately 20 Å outside the lipid bilayer (Fig. 3b). To test the function of the N-terminal region, we compared the inhibition of maltose-MBP stimulated ATPase activity by full-length $EIIA^{Glc}$ and a truncation mutant consisting of residues 19-168 (Δ1-18). The maltose transporter was reconstituted into lipid nanodiscs to allow access of MBP and $EIIA^{Glc}$ to both sides of the membrane. Both constructs of $EIIA^{Glc}$ inhibit with positive cooperativity (Fig. 3c), consistent with the 2:1 stoichiometry of the complex and an earlier observation that inhibition of maltose uptake was sigmoidally related to $EIIA^{Glc}$ concentration[24]. However, the half maximal inhibitory concentration (IC_{50}) of the Δ1-18 construct is 60 times higher than that of the full-length protein (91 μM versus 1.6 μM). This finding is consistent with the hypothesis that the full-length protein is concentrated near the membrane through the N-terminal region. Given that the intracellular concentration of $EIIA^{Glc}$ is around 50 μM[25], the membrane-anchoring function of the N-terminal region would be very important to ensure efficient inhibition of the transporter. The high IC_{50} value of the Δ1-18 construct also explains the lack of inhibition observed with a similar construct from a previous study, where the concentration used in the assay was approximately 24 μM[19].

On the basis of the structural and functional data, we propose a model for inducer exclusion of the maltose transporter (Fig. 4). The uptake and concomitant phosphorylation of glucose lead to dephosphorylation of $EIIA^{Glc}$ through a cascade of enzymes. Unphosphorylated $EIIA^{Glc}$ binds to the resting state maltose transporter and locks the MalK dimer in the open configuration. Ordinarily, binding of the maltose-loaded MBP and ATP are sufficient to

promote the transition from the inward-facing, resting state to the outward-facing, ATPase active state – the very conformational change that allows maltose entry from the periplasm and also enables ATP hydrolysis at the same time. Under inducer exclusion, $EIIA^{Glc}$ stabilizes the resting state such that MBP and ATP binding can no longer initiate the transport cycle. The maltose transporter is the only ABC transporter known to be inhibited by $EIIA^{Glc}$; however, similar allosteric regulation mechanisms by the transported substrate itself have been described for the methionine transporter and the molybdate transporter[26,27]. In both cases, at high intracellular concentrations, methionine or molybdate binds to allosteric sites in the ATPase subunits to stabilize the transporter in the inward-facing state, thus preventing further substrate uptake[26,27].

Previously it was shown that binding of $EIIA^{Glc}$ to two other transporters, LacY and MelB, were enhanced by their corresponding sugar substrates[28,29]. However, for the maltose transporter no cooperativity between substrate and $EIIA^{Glc}$ binding was observed[30]. Consistent with the functional data, the crystal structure offers no evidence that the $EIIA^{Glc}$-$MalFGK_2$ interaction would be affected by the presence of maltose. LacY and MelB are homologous proteins belonging to the major facilitator superfamily, unrelated to ABC transporters. Thus, it is likely that the mechanism underlying LacY and MelB regulation is different from that of the maltose transporter.

Methods

Expression and purification of $MalFGK_2$

Expression and purification of the maltose transporter $MalFGK_2$ with a 6×-His tag at the C-terminus of MalK were carried out as described previously[7]. In brief, the HN741 host strain [*E. coli* K-12 *argH his tpsL1 malT(Con) malBΔ13* Δ*atpBC ilv*::*Tn10/F′lacIqTn5*] containing chromosomal deletions of the genes of the maltose transport system was transformed simultaneously with three compatible antibiotic-resistance plasmids carrying *malF/malG* ($Ampicillin^R$), *malK* ($Chloramphenicol^R$) and *lacIq* ($Spectinomycin^R$). Cells were grown in Terrific Broth (Novagen) supplemented with ampicillin, chloramphenicol and spectinomycin (Sigma) at 37 °C until OD_{600} = 0.7∼0.9, and then induced with 50 μM IPTG at 22 °C for 20 hours before harvesting by centrifugation at 4,000g for 15 min. Resuspended cells were broken by two passes through a high-pressure homogenizer (Emulsiflex-C5; Avestin) and centrifuged at 80,000g for 40 min to isolate the *E. coli* membrane fraction. After resuspending the membranes in buffer containing 20 mM Tris-HCl pH 8.0, 100 mM NaCl, 5 mM $MgCl_2$, 10% glycerol, and 0.3% n-Dodecyl-β-D-Maltopyranoside (DDM, Anatrace) at a total protein concentration of 5 mg/ml, the extracted maltose transporter was purified by cobalt-affinity (Clontech) and gel filtration (Superdex 200, GE Healthcare) chromatography in buffer containing 10 mM Tris-HCl pH 8.0, 200 mM NaCl, and 0.012% DDM.

Expression and purification of $EIIA^{Glc}$

Genes encoding the full-length or (Δ1-18) $EIIA^{Glc}$ were cloned into a pMCSG7 LIC vector with a 10×-His tag followed by a TEV protease cleavage site at the N-terminus of the protein. The *E. coli* strain, BL21 Star (DE3), was transformed and grown in Luria–Bertani

medium (MP Biomedicals) at 37 °C until OD_{600} = 0.6-0.8 before induction by 100 μM IPTG at 16 °C for 20 hours. $EIIA^{Glc}$ was purified by cobalt-affinity chromatography in buffer containing 20 mM Tris-HCl pH 8.0 and 150 mM NaCl, and then incubated with TEV protease to remove the N-terminal 10×-His tag. Tag-free $EIIA^{Glc}$ was further purified by ion-exchange (Source 15Q, GE Healthcare) and gel filtration (Superdex 75, GE Healthcare) chromatography in buffer containing 10 mM Tris-HCl pH 8.0, 200 mM NaCl.

Expression and purification of MBP

Expression and purification of wild-type MBP was carried out similarly to that of $EIIA^{Glc}$ via metal affinity and gel filtration chromatography.

Crystallization of $EIIA^{Glc}$-$MalFGK_2$ complex

Preparation of a 35% bicelle stock was carried out as described previously[31,32]. In brief, 0.26 g 1,2-Dimyristoyl-sn-Glycero-3-Phosphocholine (DMPC, Avanti Polar Lipids) and 0.09 g 3-(ChlorAmidoPropyl)-dimethylammonio-2-Hydroxyl-1-Propane Sulfonate (CHAPSO, Affymetrix) were dissolved in nanopure water at a final volume of 1 ml. Multiple cycles of incubation at 42 °C, vortexing, incubation on ice, and vortexing were performed to obtain a homogeneous bicelle stock that exhibited a temperature induced phase transition between a transparent viscous gel at room temperature and a milky solution on ice. A pre-chilled protein sample containing purified $MalFGK_2$ and $EIIA^{Glc}$ at 1:2.5 molar ratio was mixed with the bicelle stock at a 4:1 ratio (v/v) on ice. The final sample for crystallization is composed of 10 mg/ml $MalFGK_2$, 2.5 mg/ml $EIIA^{Glc}$, 0.01% DDM and 7% bicelles.

Crystals were grown at 22 °C by vapor diffusion using reservoir solution containing 100 mM sodium cacodylate pH 5.6 (Sigma), 13% PEG monomethylether 2000 (Sigma) and 100 mM NDSB-256 (Non Detergent Sulfobetaine; Hampton Research). Dehydration was performed by replacing the reservoir solution every 24 hours with increasing PEG (5% per step) to a final concentration of 35%. After dehydration, crystals were looped and flash frozen in liquid nitrogen.

Data collection and structure determination

X-ray diffraction data were collected at the Advanced Photon Source (APS-23ID) at 100 K. Diffraction images were processed and scaled with HKL2000 (HKL Research, Inc.). The structure of $EIIA^{Glc}$-$MalFGK_2$ complex was solved via molecular replacement[33] (PHASER, CCP4[34]) using structures of isolated $EIIA^{Glc}$ (PDB: 1F3G)[13] and the resting state $MalFGK_2$ (PDB: 3FH6)[6]. The initial model was refined with deformable elastic network (DEN) constraints[35] in CNS[36], and then improved by cycles of manual building in COOT[37] and refinement in Phenix[38].

Reconstitution of $MalFGK_2$ into nanodiscs

Reconstitution of $MalFGK_2$ into nanodiscs was performed as described previously[39]. In brief, a lipid stock (50 mg/ml) was prepared from chloroform dissolved *E. coli* total lipids (Avanti Polar Lipids) after drying under Argon and resuspension into buffer containing 50 mM Tris-HCl pH 7.5. Dissolved lipids were purged with Argon and then sonicated to

clarity. The membrane scaffold protein (MSP) was expressed and purified as described[39]. To prepare the nanodiscs, a mixture of *E. coli* lipids, sodium cholate, purified $MalFGK_2$ and MSP at 120 μg/ml, 25 mM, 10 μM and 50 μM concentrations, respectively, was incubated at room temperature for 1 hour with gentle rocking. Nanodiscs were assembled using a 5:1 molar ratio of MSP:$MalFGK_2$ to minimize the incorporation of more than one $MalFGK_2$ complex per nanodisc. Nanodisc self-assembly was then initiated by adding hydrated Bio-Beads to remove the detergent. Bio-Beads were then removed after 3 hours of incubation at 22 °C. The mixture was loaded onto cobalt affinity resin pre-equilibrated with 20 mM Tris-HCl pH 8.0 and 100 mM NaCl. The resin was washed extensively to remove $MalFGK_2$-free nanodiscs. Nanodiscs containing $MalFGK_2$ were eluted and loaded on a desalting column to remove imidazole.

Kinetic characterization of inhibition of the maltose transporter ATPase by $EIIA^{Glc}$

The ATPase activity was determined using an ATP-regeneration/NADH-consumption coupled system[40,41] and reconstituted $MalFGK_2$ in nanodiscs. Different amounts of $EIIA^{Glc}$ were added into 100 μl reaction mixture containing 50 mM HEPES pH 8.0, 94 nM $MalFGK_2$, 15 μM MBP, 1 mM maltose, 60 μg/ml pyruvate kinase, 32 μg/ml lactate dehydrogenase, 4 mM phosphoenolpyruvate (PEP), 0.3 mM NADH and 10 mM $MgCl_2$. After incubation for 2 hours at 25 °C, 1 mM ATP was added to initiate the reaction. The absorbance at 340 nm was recorded using the 8453 UV-Vis Diode Array System (Agilent Technologies) at 25 °C for 5 minutes. All measurements were performed three times from the same protein preparations. Data were fit to either the Hill or the Michaelis-Menten equation using SigmaPlot.

Figure preparation

All structure figures were prepared with the program PyMOL (www.pymol.org).

Supplementary Material

Refer to Web version on PubMed Central for supplementary material.

Acknowledgments

We thank the staff at the Advance Photon Source GM/CA-CAT, NE-CAT and SBC for assistance with data collection. This work was supported by NIH grant (GM070515 to J.C. and A.L.D).

References

1. Gorke B, Stulke J. Carbon catabolite repression in bacteria: many ways to make the most out of nutrients. Nat Rev Microbiol. 2008; 6:613–624. [PubMed: 18628769]
2. Deutscher J, Francke C, Postma PW. How phosphotransferase system-related protein phosphorylation regulates carbohydrate metabolism in bacteria. Microbiol Mol Biol Rev. 2006; 70:939–1031. [PubMed: 17158705]
3. Wang G, Peterkofsky A, Clore GM. A novel membrane anchor function for the N-terminal amphipathic sequence of the signal-transducing protein IIAGlucose of the Escherichia coli phosphotransferase system. J Biol Chem. 2000; 275:39811–39814. [PubMed: 11044440]

4. Wang G, Keifer PA, Peterkofsky A. Solution structure of the N-terminal amphitropic domain of Escherichia coli glucose-specific enzyme IIA in membrane-mimetic micelles. Protein Sci. 2003; 12:1087–1096. [PubMed: 12717030]
5. Hogema BM, et al. Inducer exclusion in Escherichia coli by non-PTS substrates: the role of the PEP to pyruvate ratio in determining the phosphorylation state of enzyme IIAGlc. Mol Microbiol. 1998; 30:487–498. [PubMed: 9822815]
6. Khare D, Oldham ML, Orelle C, Davidson AL, Chen J. Alternating access in maltose transporter mediated by rigid-body rotations. Mol Cell. 2009; 33:528–536. [PubMed: 19250913]
7. Oldham ML, Khare D, Quiocho FA, Davidson AL, Chen J. Crystal structure of a catalytic intermediate of the maltose transporter. Nature. 2007; 450:515–521. [PubMed: 18033289]
8. Oldham ML, Chen J. Crystal structure of the maltose transporter in a pretranslocation intermediate state. Science. 2011; 332:1202–1205. [PubMed: 21566157]
9. Monod J, Wyman J, Changeux JP. On the Nature of Allosteric Transitions: A Plausible Model. J Mol Biol. 1965; 12:88–118. [PubMed: 14343300]
10. Chen J, Lu G, Lin J, Davidson AL, Quiocho FA. A tweezers-like motion of the ATP-binding cassette dimer in an ABC transport cycle. Mol Cell. 2003; 12:651–661. [PubMed: 14527411]
11. Dean DA, Reizer J, Nikaido H, Saier MH Jr. Regulation of the maltose transport system of Escherichia coli by the glucose-specific enzyme III of the phosphoenolpyruvate-sugar phosphotransferase system. Characterization of inducer exclusion-resistant mutants and reconstitution of inducer exclusion in proteoliposomes. J Biol Chem. 1990; 265:21005–21010. [PubMed: 2250006]
12. Kuhnau S, Reyes M, Sievertsen A, Shuman HA, Boos W. The activities of the Escherichia coli MalK protein in maltose transport, regulation, and inducer exclusion can be separated by mutations. J Bacteriol. 1991; 173:2180–2186. [PubMed: 2007546]
13. Worthylake D, et al. Three-dimensional structure of the Escherichia coli phosphocarrier protein IIIglc. Proc Natl Acad Sci U S A. 1991; 88:10382–10386. [PubMed: 1961703]
14. Cai M, et al. Solution structure of the phosphoryl transfer complex between the signal-transducing protein IIAGlucose and the cytoplasmic domain of the glucose transporter IICBGlucose of the Escherichia coli glucose phosphotransferase system. J Biol Chem. 2003; 278:25191–25206. [PubMed: 12716891]
15. Hurley JH, et al. Structure of the regulatory complex of Escherichia coli IIIGlc with glycerol kinase. Science. 1993; 259:673–677. [PubMed: 8430315]
16. Wang G, et al. Solution structure of the phosphoryl transfer complex between the signal transducing proteins HPr and IIA(glucose) of the Escherichia coli phosphoenolpyruvate:sugar phosphotransferase system. EMBO J. 2000; 19:5635–5649. [PubMed: 11060015]
17. Pelton JG, Torchia DA, Meadow ND, Roseman S. Structural comparison of phosphorylated and unphosphorylated forms of IIIGlc, a signal-transducing protein from Escherichia coli, using three-dimensional NMR techniques. Biochemistry. 1992; 31:5215–5224. [PubMed: 1606145]
18. Dorschug M, Frank R, Kalbitzer HR, Hengstenberg W, Deutscher J. Phosphoenolpyruvate-dependent phosphorylation site in enzyme IIIglc of the Escherichia coli phosphotransferase system. Eur J Biochem. 1984; 144:113–119. [PubMed: 6383826]
19. Bluschke B, Volkmer-Engert R, Schneider E. Topography of the surface of the signal-transducing protein EIIA(Glc) that interacts with the MalK subunits of the maltose ATP-binding cassette transporter (MalFGK2) of Salmonella typhimurium. J Biol Chem. 2006; 281:12833–12840. [PubMed: 16527815]
20. Stein A, et al. Functional characterization of the maltose ATP-binding-cassette transporter of Salmonella typhimurium by means of monoclonal antibodies directed against the MalK subunit. Eur J Biochem. 2002; 269:4074–4085. [PubMed: 12180984]
21. Meadow ND, Roseman S. Sugar transport by the bacterial phosphotransferase system. Isolation and characterization of a glucose-specific phosphocarrier protein (IIIGlc) from Salmonella typhimurium. J Biol Chem. 1982; 257:14526–14537. [PubMed: 6754734]
22. Meadow ND, Savtchenko RS, Remington SJ, Roseman S. Effects of mutations and truncations on the kinetic behavior of IIAGlc, a phosphocarrier and regulatory protein of the

phosphoenolpyruvate phosphotransferase system of Escherichia coli. J Biol Chem. 2006; 281:11450–11455. [PubMed: 16439362]

23. Misko TP, Mitchell WJ, Meadow ND, Roseman S. Sugar transport by the bacterial phosphotransferase system. Reconstitution of inducer exclusion in Salmonella typhimurium membrane vesicles. J Biol Chem. 1987; 262:16261–16266. [PubMed: 3316216]
24. van der Vlag J, van Dam K, Postma PW. Quantification of the regulation of glycerol and maltose metabolism by IIAGlc of the phosphoenolpyruvate-dependent glucose phosphotransferase system in Salmonella typhimurium. J Bacteriol. 1994; 176:3518–3526. [PubMed: 8206828]
25. Scholte BJ, Schuitema AR, Postma PW. Isolation of IIIGlc of the phosphoenolpyruvate-dependent glucose phosphotransferase system of Salmonella typhimurium. J Bacteriol. 1981; 148:257–264. [PubMed: 7026533]
26. Kadaba NS, Kaiser JT, Johnson E, Lee A, Rees DC. The high-affinity E. coli methionine ABC transporter: structure and allosteric regulation. Science. 2008; 321:250–253. [PubMed: 18621668]
27. Gerber S, Comellas-Bigler M, Goetz BA, Locher KP. Structural basis of trans-inhibition in a molybdate/tungstate ABC transporter. Science. 2008; 321:246–250. [PubMed: 18511655]
28. Osumi T, Saier MH Jr. Mechanism of regulation of the lactose permease by the phosphotransferase system in Escherichia coli: evidence for protein-protein interaction. Ann Microbiol (Paris). 1982; 133:269–273. [PubMed: 7044217]
29. Osumi T, Saier MH Jr. Regulation of lactose permease activity by the phosphoenolpyruvate:sugar phosphotransferase system: evidence for direct binding of the glucose-specific enzyme III to the lactose permease. Proc Natl Acad Sci U S A. 1982; 79:1457–1461. [PubMed: 7041121]
30. Saier MH Jr, Novotny MJ, Comeau-Fuhrman D, Osumi T, Desai JD. Cooperative binding of the sugar substrates and allosteric regulatory protein (enzyme IIIGlc of the phosphotransferase system) to the lactose and melibiose permeases in Escherichia coli and Salmonella typhimurium. J Bacteriol. 1983; 155:1351–1357. [PubMed: 6350268]

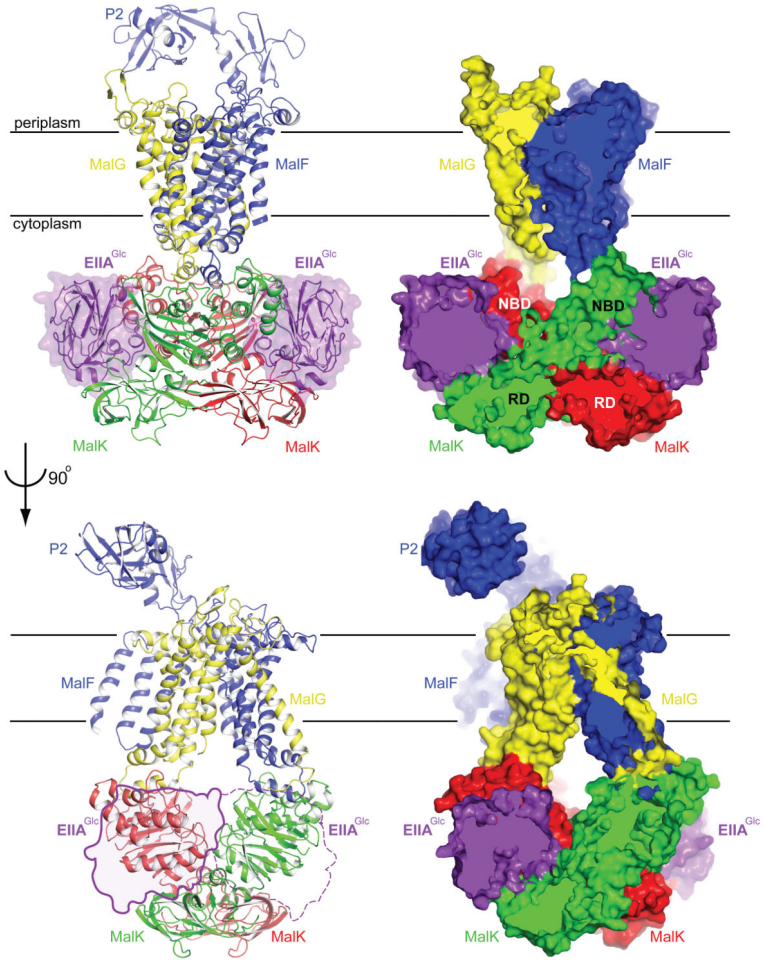

Figure 1. Two orthogonal views of the EIIA^{Glc}-MalFGK$_2$ complex

Both a ribbon diagram (left) and a slab view (right) are shown. In the lower panel, EIIA^{Glc} is represented by a transparent surface, with the solid line representing the front molecule and dotted line representing the backside one.

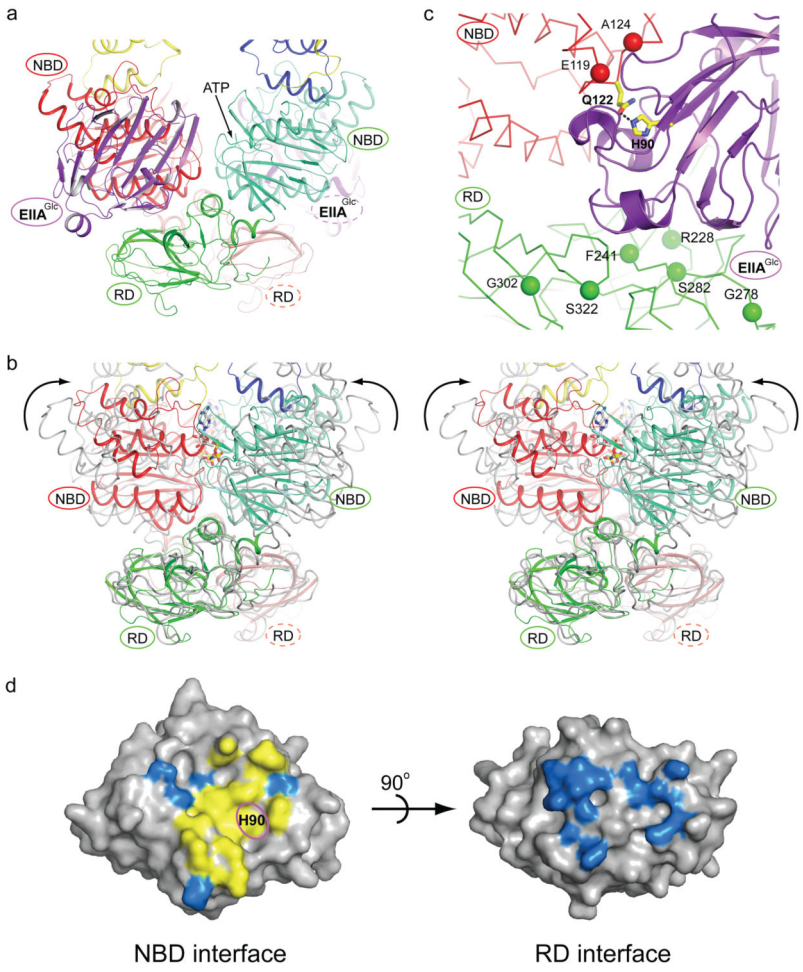

Figure 2. Binding of EIIA^{Glc} prevents MalK closure

a, MalK dimer bound with EIIA^{Glc}. EIIA^{Glc} is shown in purple. The two MalK subunits are coloured in red and green. The nucleotide binding domain (NBD) and regulatory domain (RD) within each MalK subunit are rendered in different shades. The ATP binding site (the Walker A motif) in the front subunit (green) is indicated by an arrow. **b,** Stereoview of a superposition of the closed MalK dimer, coloured as in panel a, with the open dimer coloured in grey. ATP is shown in stick model. The arrows indicate the rotations of the NBDs necessary to form the closed dimer. **c,** EIIA^{Glc}-MalK interface. Inducer exclusion resistant mutants are labeled. The active site His 90 of EIIA^{Glc} and Gln 122 of MalK are shown in stick models, and the Hydrogen bond between His 90 and Gln 122 is indicated by a dashed line. **d,** Surface presentations of EIIA^{Glc}. Residues located within 4.5 Å from the NBD (left) or RD (right) are coloured. Yellow, the 11 residues (Val 39, Val 40, Phe 41, Ile 45, Val 46, Lys 69, Phe 71, Glu 72, Phe 88, His 90, and Val 96) involved in interacting with all four EIIA^{Glc} partners: MalK, glycerol kinase, HPr, and EIIB^{Glc}. The phosphorylation site His 90 is labeled. Blue, MalK interacting residues that are not part of the canonical binding surface

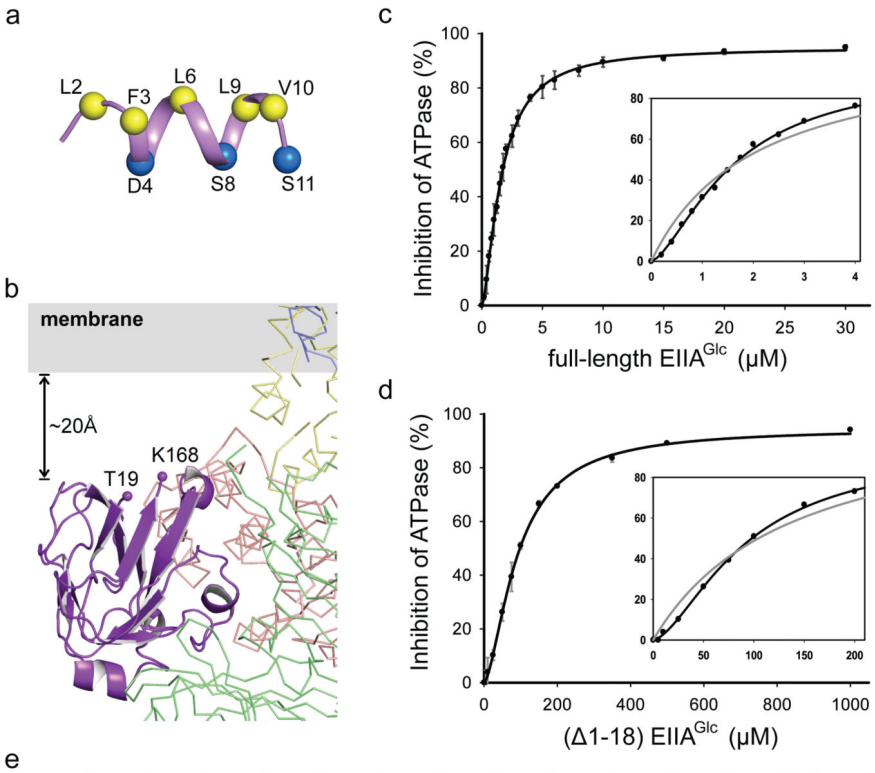

e

	full-length EIIA^{Glc}	(Δ1-18)EIIA^{Glc}
IC_{50} (μM)	1.61 ± 0.04	91 ± 3
Hill coefficient	1.53 ± 0.05	1.60 ± 0.08
Max. Inhibition (%)	95 ± 1	94.7 ± 1.9

Figure 3. The N-terminus of EIIA^{Glc} likely functions as a membrane anchor

a, Structure of the N-terminal peptide determined by NMR in dihexanoyl phosphatidylglycerol (PDB 1O53)[4]. Hydrophobic residues lining one side of the helix are shown in yellow. Hydrophilic residues on the opposite side of the helix are shown in blue. **b,** Close-up view of EIIA^{Glc} bound to MalK. The two terminal residues visible in the crystal structure (Thr 19 and Lys 168) are labeled. **c,d,** Inhibition of the MBP-stimulated ATPase activity of reconstituted nanodiscs by full-length **(c)** and N-terminal truncated EIIA^{Glc} **(d)**. Data points represent the means ± standard deviation of triplicate measurements. Insets show enlargements of the figures fitted to the Hill equation (black line) and to the Michaelis-Menten equation (grey line). **e,** Summary table of the kinetics.

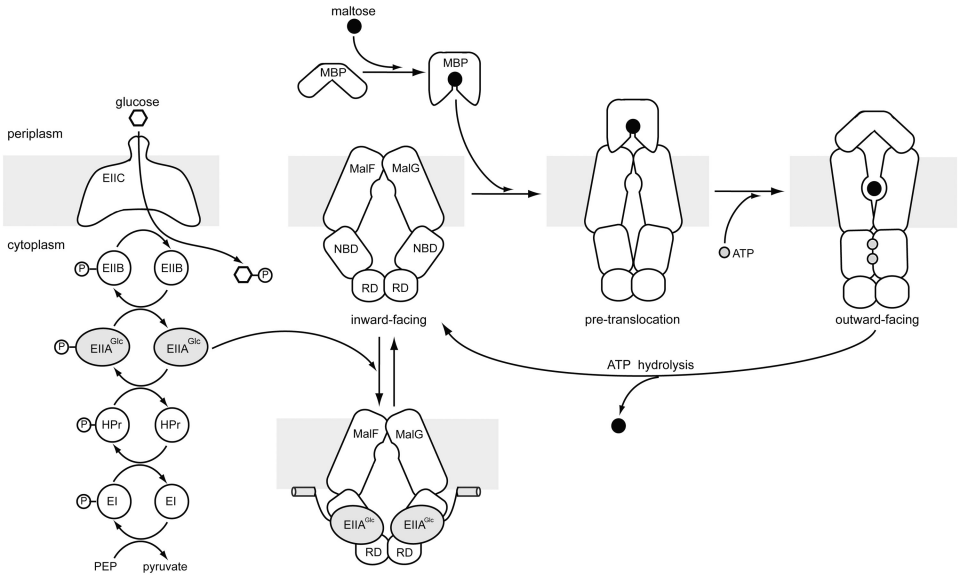

Figure 4. Inhibition of the maltose transporter by inducer exclusion

Left, Glucose and other PTS substrates are transported and phosphorylated by five coupled reactions, leading to an increased level of unphosphorylated $EIIA^{Glc}$. **Right,** the maltose transport cycle. In the resting state, the open MalK dimer coincides with the inward-facing TM domains. Upon association of MBP, the transporter undergoes a conformational change (the pre-translocation state) that permits ATP to promote a concerted motion of MalK closure, reorientation of the TM domains, and opening of MBP. Formation of the outward-facing conformation transfers maltose from MBP to the TM binding site, and at the same time positions ATP at the catalytic site for hydrolysis. ATP hydrolysis releases maltose into the cytoplasm and resets the transporter to the resting state. Under conditions subject to inducer exclusion, unphosphorylated $EIIA^{Glc}$ binds and stabilizes the resting state transporter, thus inhibiting maltose transport.